Reconstruction of objects with a limited number of non-zero components in fluorescence microscopy

Brynmor J. Davis[a], William C. Karl[a], Anna K. Swan [a], Bennett B. Goldberg[b,a], M. Selim Ünlü[a] and Marcia B. Goldberg[c]

[a] Department of Electrical and Computer Engineering, Boston University, 8 St. Mary's Street, Boston, MA 02215, USA;

[b] Department of Physics, Boston University, 590 Commonwealth Avenue, Boston, MA 02215, USA;

[c] Infectious Disease Division, Massachusetts General Hospital, University Park, 65 Landsdowne Street, Cambridge, MA 02139, USA

ABSTRACT

A reconstruction algorithm is developed that uses specific a-priori knowledge to produce higher resolution images than standard approaches. Deconvolution is an important image reconstruction tool in fluorescence microscopy. This is especially true for modern interferometric instruments (such as I^5M and 4Pi systems), as they may have complicated oscillatory point spread functions. Current methods are designed to work on an arbitrary object — i.e. it is assumed that there is no available a-priori knowledge of the object (with the possible exception of a non-negative condition on the fluorophore-emission intensities). In situations where there is a-priori knowledge of the object, it may be possible to use this information to produce a higher quality reconstruction of the object. A useful a-priori condition is investigated here.

It is assumed that the object can be represented by the sum of not more than L basis functions. The simplest example of this is when the basis functions are impulses — this leads to an object of L or less non-zero points on a background of zeros. This a-priori condition can be applied directly; applied to a limited region of the object; applied in one dimension (for an object with a layered structure such as lipid bilayers); or applied in two dimensions (for an object with a filamentary structure such as actin fibers.) A reconstruction algorithm is described and applied to some illustrative simulated examples. The results are found for several fluorescence microscopy methodologies and compared to the results produced by standard deconvolution methods.

Keywords: Fluorescence microscopy, deconvolution, prior knowledge, image reconstruction, super-resolution

1. INTRODUCTION

Deconvolution is an integral and well-studied[1–4] part of modern fluorescence microscopy. Processing of the raw data is necessary to ensure that the maximum achievable image resolution is realized. In fact, the newer interferometric methodologies[5,6] rely on deconvolution as a fundamental step in their operation rather than just a method of sharpening the raw data. Image reconstruction algorithms can also be used ensure that the resulting image conforms to any a-prior knowledge of the object. The most commonly used prior in fluorescence microscopy is non-negativity — it is not physically possible for the fluorophore density to be negative.

A much stronger prior will be used here. This means that the resulting algorithm will not be as widely applicable but it does give the potential to achieve higher resolutions in scenarios where the prior is met. The prior restriction will be that the imaged fluorophore density is constructed from a weighted sum of L (or less) known basis densities. This obviously means that an arbitrary non-negative fluorophore density can not be reconstructed as is the case with most other reconstruction approaches.

The next section outlines the physics assumed in the imaging process. Some useful basis densities are then discussed, followed by a development of the algorithm. Some simple examples are given to motivate the use of this approach. Conclusions and references end the paper.

Correspondence to Brynmor Davis (bryn@bu.edu)

2. THE OBSERVATION MODEL

The majority of three-dimensional fluorescence microscopy instruments are linear and shift invariant, which means that the data produced can be related to the object investigated by a convolution equation.

$$d(x,y,z) = \int\int\int h(x-x',y-y',z-z')o(x',y',z')dx'dy'dz' \quad + \quad n(x,y,z) \tag{1}$$

Here the data $d(x,y,z)$ is related to the object $o(x,y,z)$ through a convolution with the instrument's point spread function $h(x,y,z)$. All noise effects are assumed additive and included in the function $n(x,y,z)$. Equation 1 is the starting point for any physically-based procedure for constructing an estimate of the object.

It will be assumed here that the object can be written as follows.

$$o(x,y,z) = \sum_{i=1}^{N} \alpha_i \, b_i(x,y,z) \tag{2}$$

This equation states that the object is the weighted sum of some set of basis functions $\{b_i(x,y,z)\}$ (possible choices of these basis functions are discussed in the next section). Additionally, it will be assumed that not more than L of the α_i coefficients are non-zero but it is not known which L this is. If the α_i coefficients are collected into a vector α then this condition can be stated as follows

$$\|\alpha\|_0 \leq L \tag{3}$$

Where $\|\cdot\|_0$ represents the common ℓ_0-norm* and simply counts the number of non-zero components.

Inserting Equation 2 into Equation 1 gives the following result.

$$\begin{aligned} d(x,y,z) &= \sum_{i=1}^{N} \alpha_i \int\int\int h(x-x',y-y',z-z')b_i(x',y',z')dx'dy'dz' \quad + \quad n(x,y,z) \\ &= \sum_{i=1}^{N} \alpha_i \, g_i(x,y,z) \quad + \quad n(x,y,z) \end{aligned} \tag{4}$$

This is the new observation equation. The reconstruction problem will be to find the L non-zero α_is from the data $d(x,y,z)$.

3. USEFUL BASES

The basis functions $b_i(x,y,z)$ represent the fluorophore densities that may be present in the object. In general the basis functions chosen to represent the object will depend strongly on what type of specimen is being imaged. Several potentially useful possibilities will be discussed here.

3.1. Impulses

If the object is believed to have not more than L non-zero points then the obvious choice of basis is impulses.

$$b_i(x,y,z) = \delta(x-x_i, y-y_i, z-z_i) \tag{5}$$

The i^{th} impulse is located at (x_i, y_i, z_i). In choosing these locations, a discrete space representation of the object is implied (as the object can only be non-zero on a discrete set of N locations). When α is recovered it simply gives pixel values at a set of L positions.

*Strictly speaking, this is not a norm as it violates the axiom $\|kx\| = |k| \, \|x\|$ (where x is a vector and k is a scalar).

3.2. Lines

Consider a basis set comprising of straight lines (with constant fluorophore density along the lines) of various offset and inclination. While it is unlikely that many real three-dimensional specimens could be constructed from such a basis (as filamentary fibers will almost certainly bend and have a non-constant fluorophore density along a strand), the basis can still find use. Consider a two-dimensional plane of data resulting from imaging actin fibers. The volume of the object that contributes to this data is a planar slice with thickness determined by the width of the point spread function. Over this volume it may be sufficiently accurate to model the actin fibers as a sum of constant, straight lines. This means that if an inversion is performed on the 2D plane of data, then the resulting L non-zero α_i coefficients would determine the fluorophore density and select the offset and the orientation of the fibers as they passed through the plane.

This could be done plane-by-plane to build up a full 3D image. Continuity between the planes would not be guaranteed though. To achieve this sort of continuity, a more complicated set of basis functions would be required. They would have to take into account fiber bending and non-uniform fluorophore distribution over the fibers.

3.3. Planes

This is a similar idea to the 'lines' basis except now constant-fluorophore-density planes of varying offset and inclination are used. If a one-dimensional line of data is taken, a tubular volume of the object (with width and breadth again determined by the point-spread function) contributes to this data. If an object such as lipid-bilayers/cell-walls can be modeled as locally planar in this region, then the local planar properties can be found by finding the appropriate α for the line of data. An example of this idea is shown in Section 5.

4. THE RECONSTRUCTION PROCESS

The critical problem is determining the coefficient vector α from the data given. A standard approach in these sorts of inversion problems is to select the minimum-square-error solution — that is, the one that minimizes the square difference between the actual data and the data that would be expected. That is what will be done here with the additional constraint that not more than L of the α_i terms are non-zero and that none are negative. It will be assumed that the basis functions are non-negative so that the final constraint ensures a non-negative solution. This reconstruction rule is thus written as follows.

$$\hat{\alpha} = \underset{\alpha}{\operatorname{argmin}} \left\{ \| d(x,y,z) - \sum_{i=1}^{N} \alpha_i \, g_i(x,y,z) \|_2 \right\} \quad s.t. \quad \|\alpha\|_0 \leq L, \; \alpha_i \geq 0 \tag{6}$$

Where $\| \cdot \|_2$ represents the standard ℓ_2 norm. This type of decision criterion is known as ℓ_0–regularization (after the norm used) and is currently an active topic of investigation in the signal processing community.[7–9] These investigations have produced results concerning (amongst other things) the uniqueness of ℓ_0 solutions, computationally efficient solution methods and noise stability bounds. Rather than reproducing these results here, a general discussion of ℓ_0–reconstruction and a demonstration of some achievable results will be presented.

To solve Equation 6 consider an exhaustive search over all possible combinations of L basis vectors. That is, examine each possible set of L basis vectors from the complete set of N and select the one that allows the least square-error. Let I_j indicate the j^{th} set of possible non-zero indices (so that I_j contains L numbers between 1 and N inclusive). There are N-choose-L possible I_js. For each one, the best coefficient values and the resulting cost will be found. The best coefficients $\hat{\alpha}^j$ satisfy the following equation.

$$\hat{\alpha}^j = \underset{\alpha}{\operatorname{argmin}} \left\{ \| d(x,y,z) - \sum_{i \in I_j} \alpha_i \, g_i(x,y,z) \|_2 \right\} \quad s.t. \quad \alpha_i \geq 0 \tag{7}$$

This is a standard problem and can be easily solved. The final reconstruction is found by simply comparing the costs for all I_j and selecting the minimum.

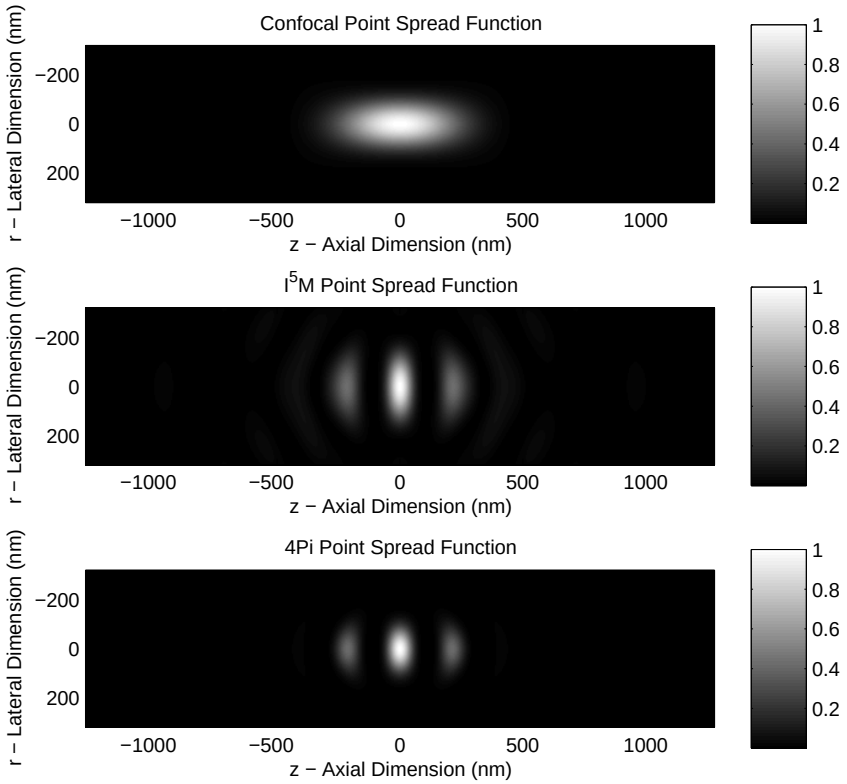

Figure 1. Point spread functions for the three instruments investigated — confocal, I^5M and 4Pi. Note that the three-dimensional responses are rotationally symmetric about the z axis which means the above images completely specify the 3D point spread functions. The axial dimension (z) is along the optic axis while the lateral dimension ($r = \sqrt{x^2 + y^2}$) is parallel to the focal plane.

Note that the cost of this method increases very rapidly with L (combinatorically in fact). Faster methods are possible[8] but the brute force approach guarantees the best solution without getting mired in implementation issues. The computational cost may be a limiting factor in certain applications but certain easy steps can be taken. For example, a standard reconstruction may be used to get an idea of where the components of interest are. Only I_j sets that are consistent with this may be tested (i.e. the components are localized to a general area using a standard reconstruction and the ℓ_0 approach is applied over only these areas to refine the resolution).

5. EXAMPLES

This section applies the algorithm developed to some simulated data for confocal, I^5M and 4Pi systems. The point spread functions for these systems were calculated as in Ref. 10 — i.e. using the vectoral theory of Ref. 11 and with numerical aperture of 1.35, index of refraction of 1.51, an excitation wavelength of 488nm and a detection wavelength of 500nm. The point spread functions were calculated on a 5nm grid. Figure 1 shows the resulting functions. The object to be imaged will be assumed to have planes perpendicular to the optic axis. A one-dimensional scan through these planes will be taken and an axial profile estimated from this. The basis functions $\{b_i(x, y, z)\}$ will be a collection of planes parallel to the focal plane.

$$b_i(x, y, z) = \delta(z - z_i) \tag{8}$$

Equation 4 gives the general observation equation. For this basis the following can be easily shown.

$$d(z) = \sum_{i=1}^{N} \alpha(z_i) g(z - z_i) \quad where \quad g(z) = \int\int h(x, y, z)\, dx\, dy \tag{9}$$

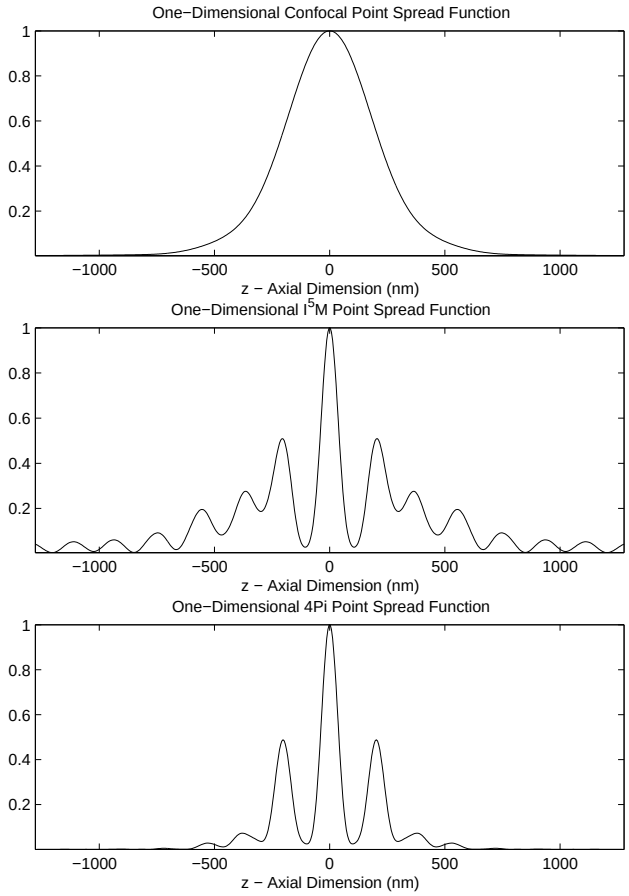

Figure 2. One-dimensional point spread functions for the three instruments (confocal, I^5M and 4Pi) investigated.

Here α_i and $g_i(x, y, z)$ have been indexed by z_i so that the data can be cast as a one-dimensional convolution. The effect of the planes in the object is to integrate the point spread function in the lateral dimensions. Figure 2 shows the one-dimensional point spread functions $g(z)$.

Several two-layer objects will be simulated to demonstrate the reconstruction method described here. The results will be compared to a standard Tikhonov reconstruction[12] with a non-negativity condition enforced. Tikhonov reconstruction is a minimum-least-square-error method with an additional term to eliminate instability due to noise. Applied to the same variables as Equation 6, Tikhonov reconstruction is the following.

$$\hat{\alpha} = \underset{\alpha}{\operatorname{argmin}} \left\{ \|d(x, y, z) - \sum_{i=1}^{N} \alpha_i \, g_i(x, y, z)\|_2^2 + \gamma^2 \|\alpha\|_2^2 \right\} \quad s.t. \quad \alpha_i \geq 0 \tag{10}$$

This reconstruction is easily implemented and computationally efficient.

The first object will have two equal-fluorophore-density layers separated by 200nm. The data is contaminated with Poisson noise[†] and has a maximum photon count of approximately 150. Figure 3 shows the resulting Tikhonov and two-layer reconstructions. The Tikhonov regularization parameter γ was chosen manually as a balance between resolving the two layers and removing noise artifacts. It can be seen that in all three cases the Tikhonov reconstruction resolves the two layers. However, it does lower and spread the fluorophore density to

[†]The minimum-square-error condition used in this paper is matched to constant-variance Gaussian noise rather than Poisson noise. Methods specific to Poisson statistics do exist[13] but the minimum-square-error method has been used here for simplicity.

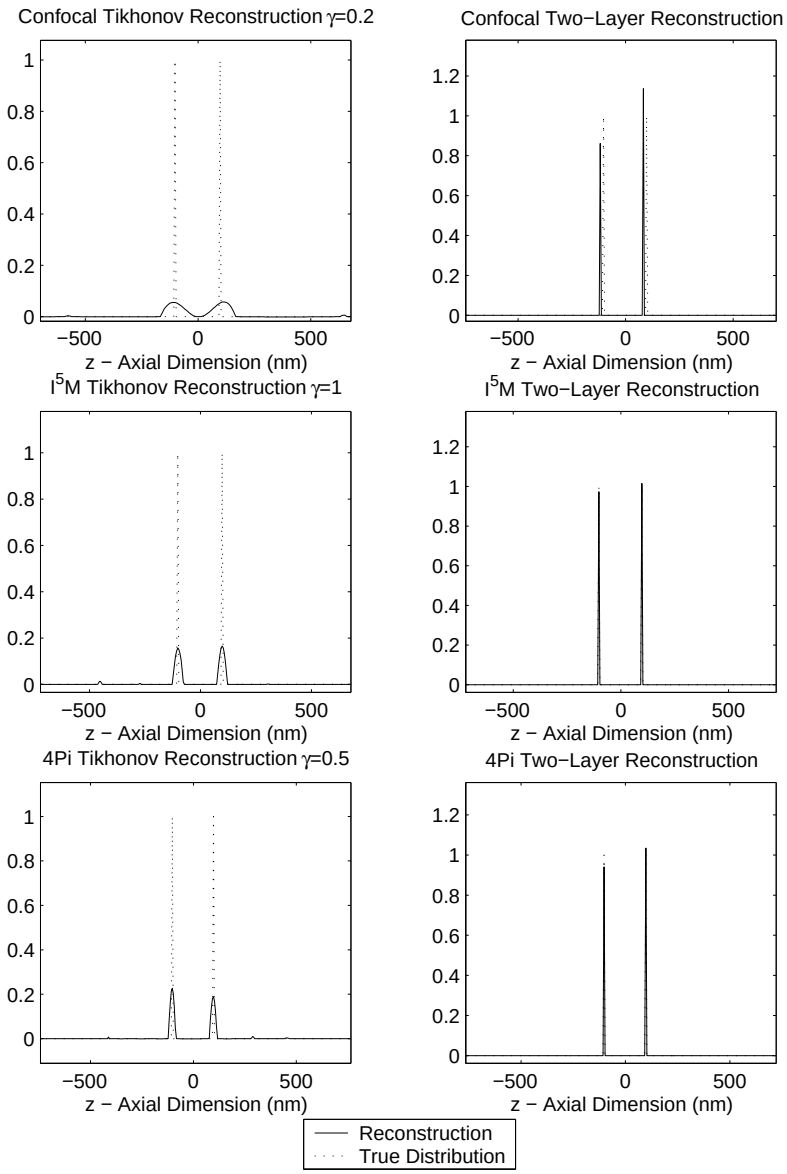

Figure 3. Tikhonov and two-layer (L=2) reconstructions for confocal, I^5M and 4Pi data. The two layers are separated by 200nm.

a greater or lesser extent. This problem does not occur with the two-layer reconstructions. Note that a 200nm separation is about as narrow of a gap as can be reliably reconstructed for confocal data (at this noise level) using the algorithm described in this paper. Notice that the positioning of the two layers is not exact for the confocal case. Obviously, reconstructions with more than two layers would perform even more poorly. The 4Pi and I^5M reconstructions worked very well.

Figure 4 shows a scenario with a closer layer spacing (20nm) and a better signal-to-noise ratio (in this case the maximum count is approximately 2000). The 20nm spacing is well below the accepted resolution of any of these instruments and as expected, the Tikhonov reconstruction method fails to resolve the layers in all cases. The two-layer algorithm fails for the confocal case (choosing a strong central peak rather than two of even density). However, both the I^5M and 4Pi reconstructions are accurate. This shows that with the appropriate prior knowledge, it is possible to see detail below the accepted resolution limit.

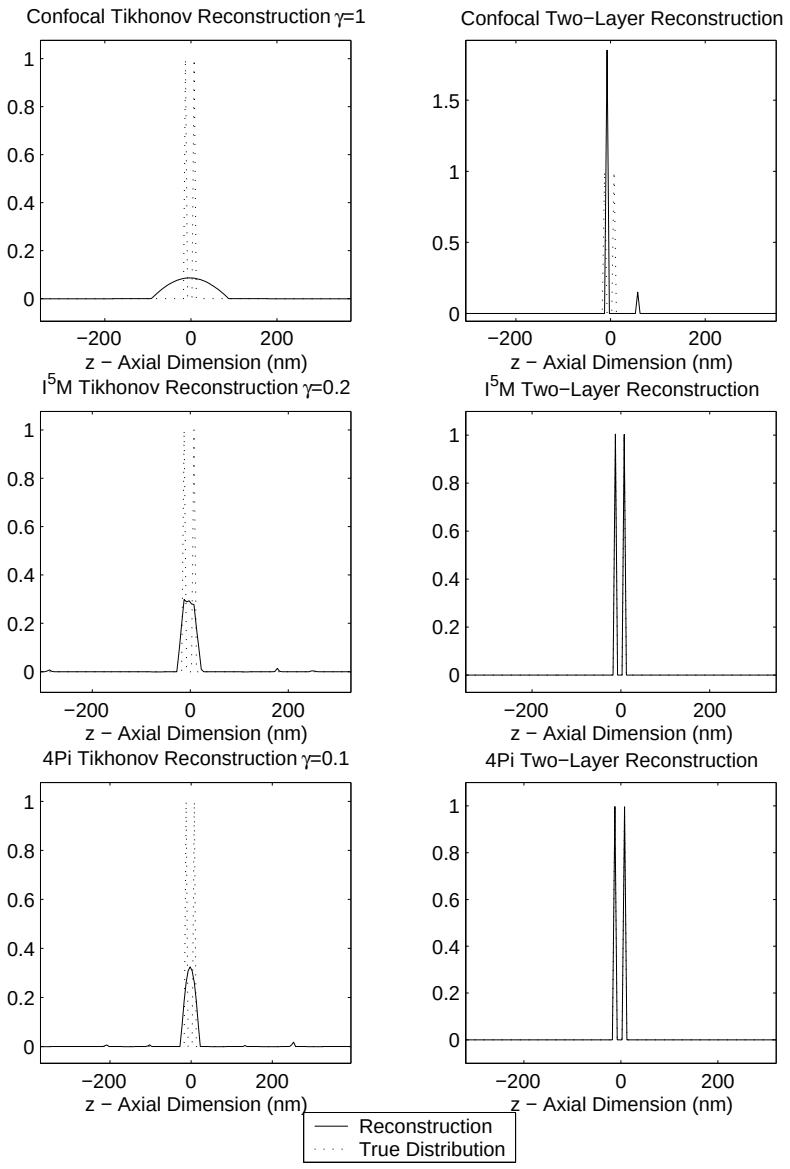

Figure 4. Tikhonov and two-layer (L=2) reconstructions for confocal, I^5M and 4Pi data. The two layers are separated by 20nm.

6. CONCLUSIONS

A deconvolution algorithm has been described that allows only a limited number of non-zero components in the reconstructed image. The components are basis functions that are chosen by the user. Examples have shown that (at least in some simple cases) there is scope for a significant increase in resolution if the object is consistent with the condition on the number of components. However, the major drawback of the algorithm is that an exhaustive search technique is used. More efficient implementations are a possible path of future research. The results presented here also show that there is potential for strong prior knowledge to improve the resolution[‡] of an instrument.

[‡]The term 'resolution' should be used with care in this type of non-linear reconstruction process as the image quality is dependent on the object.

REFERENCES

1. W. A. Carrington, R. M. Lynch, E. D. W. Moore, G. Isenberg, K. E. Fogarty, and F. S. Fay, "Superresolution three-dimensional images of fluorescence in cells with minimal light exposure," *Science* **268**, pp. 1483–1487, June 1995.
2. J.-A. Conchello and J. G. McNally, "Fast regularization technique for expectation maximization algorithm for optical sectioning microscopy," in *Three-Dimensional Microscopy: Image Aquisition and Processing III*, C. J. Cogswell, G. S. Kino, and T. Wilson, eds., *Proc. SPIE* **2655**, pp. 199–208, 1996.
3. P. J. Verveer, M. J. Gemkow, and T. M. Jovin, "A comparison of image restoration approaches applied to three-dimensional confocal and wide-field fluorescence microscopy," *J. Microsc.* **193**, pp. 50–61, January 1999.
4. M. Nagorni and S. W. Hell, "Coherent use of opposing lenses for axial resolution increase. II. Power and limitation of nonlinear image restoration," *J. Opt. Soc. Am. A* **18**, pp. 49–54, January 2001.
5. S. Hell and E. H. K. Stelzer, "Properties of a 4Pi confocal fluorescence microscope," *J. Opt. Soc. Am. A* **9**, pp. 2159–2166, December 1992.
6. M. G. L. Gustafsson, D. A. Agard, and J. W. Sedat, "Sevenfold improvement of axial resolution in 3D widefield microscopy using two objective lenses," in *Three-Dimensional Microscopy: Image Aquisition and Processing II*, T. Wilson and C. J. Cogswell, eds., *Proc. SPIE* **2412**, pp. 147–156, 1995.
7. D. Donoho and X. Huo, "Uncertainty principles and ideal atomic decomposition," *IEEE Trans. Inform. Theory* **47**, pp. 2845–2862, November 2001.
8. D. Donoho and M. Elad, "Optimally sparse representation in general (non-orthogonal) dictionaries via ℓ^1 minimization," 2002. www-stat.stanford.edu/~donoho/reports.html.
9. B. Wohlberg, "Noise sensitivity of sparse signal representations: Reconstruction error bounds for the inverse problem," *IEEE Trans. Signal Processing* **51**, pp. 3053–3060, December 2003.
10. M. Nagorni and S. Hell, "Coherent use of opposing lenses for axial resolution increase in fluorescence microscopy. I Comparitive study of concepts," *J. Opt. Soc. Am. A* **18**, pp. 36–48, January 2001.
11. B. Richards and E. Wolf, "Electromagnetic diffraction in optical systems. II. Structure of the image field in an aplanatic system," *Proc. R. Soc. London, Ser. A* **253**, pp. 358–379, 1959.
12. H. Engl, M. Hanke, and A. Neubauer, *Regularization of Inverse Problems*, Kluwer Academic Publishers, 1996.
13. L. B. Lucy, "An iterative technique for the rectification of observed distributions," *Astron. J.* **79**, pp. 745–754, June 1974.